International Journal of Nanoelectronics and Materials
IJNeaM
ISSN 1985-5761 | E-ISSN 2232-1535

Optimization of silver nanoparticles synthesis: effects of trisodium citrate parameters and reaction temperature

Nur Atiqah Azman [a], Nor Shahanim Mohamad Hadis [a] *, Ahmad Al-Amin Ahamad Husaini [a], Mohamad Faizal Abd Rahman [a], Zurita Zulkifli [b], Anis Diyana Rosli [a], Aida Zulia Zulhanip [a]

[a]*Electrical Engineering Studies, Universiti Teknologi MARA, Cawangan Pulau Pinang, 13500 Permatang Pauh, Pulau Pinang, Malaysia*
[b]*School of Electrical Engineering, College of Engineering, Universiti Teknologi MARA, 40450 Shah Alam, Selangor Darul Ehsan, Malaysia*
** Corresponding author. Tel.: +60-382-2788; fax: +0-000-000-0000; e-mail: norsh713@uitm.edu.my*

Received 9 April 2025, Revised 19 December 2025, Accepted 19 March 2026

ABSTRACT

Silver nanoparticles (AgNPs) exhibit unique optical and chemical properties that enable broad applications in sensing, catalysis, and nanomedicine. This study optimized AgNPs synthesis using the Turkevich method, in which silver nitrate ($AgNO_3$) serves as the silver precursor and trisodium citrate (TSC) acts as both the reducing and stabilizing agent. The effects of a fixed $AgNO_3$ concentration of 0.034 g (0.06 mM), TSC addition timing, storage conditions, reaction temperatures of 70°C, 80°C, and 90°C, and TSC concentrations of 0.5 g (0.136 mM), 1.0 g (0.272 mM), and 1.5 g (0.408 mM) were investigated. Characterization using FESEM and EDX, UV-VIS spectroscopy, Zeta Potential, and Zeta Sizer (dynamic light scattering, DLS) revealed that higher temperatures (≥80°C) combined with higher TSC concentrations of 1.0 g and 1.5 g produced smaller, more stable nanoparticles of 72.85–90.38 nm with a polydispersity index (PdI) of 0.5–0.7, indicating good uniformity. UV-VIS spectra confirmed AgNPs formation, with surface plasmon resonance peaks at 436–519 nm. Zeta potential values below –40 mV at higher TSC concentrations indicated excellent colloidal stability, whereas lower temperatures and insufficient TSC led to aggregation. Storage at room temperature accelerated oxidation and particle growth. Optimal synthesis conditions of 80°C to 90°C with 1.0 g to 1.5 g of TSC offer a reproducible method for fabricating stable AgNPs.

Keywords: *Turkevich method, FESEM, EDX, UV-VIS spectroscopy, Zeta potential, Polydispersity index (PDI), Colloidal stability*

1. INTRODUCTION

Silver nanoparticles (AgNPs) have gained significant attention due to their unique physicochemical properties, including localized surface plasmon resonance (LSPR), high electrical conductivity, and antimicrobial activity [1]. Their tunable optical properties, influenced by size, shape, and aggregation, make them highly effective in sensing applications, such as surface-enhanced Raman scattering (SERS) and colorimetric detection of environmental pollutants like heavy metals [2, 3]. The antimicrobial performance of AgNPs, dependent on morphology and surface coatings, has also led to applications in medical devices and antiseptics [4, 5]. These versatile properties support their widespread use in diagnostics, therapeutics, catalysis, and consumer products [1, 6].

In catalysis, AgNPs facilitate organic pollutant degradation due to their redox properties, though efficiency is influenced by surface chemistry and stabilizers [5]. In heavy metal detection, AgNPs-based sensors exploit LSPR shifts and electrochemical enhancements for high sensitivity. Pb^{2+} detection utilizes LSPR peak shifts from nanoparticle aggregation, causing visible colour changes on cellulose strips [3]. Similarly, Hg^{2+} sensing relies on AgNPs-based plasmonic signal quenching or enhancement, enabling high selectivity in water with detection limits in the low ppb range [7, 8]. These remarkable sensing capabilities stem from AgNPs' high electron transfer rates and surface reactivity, enhancing signal amplification in optical and electrochemical platforms [8, 9].

Among various synthesis techniques, the Turkevich method is widely employed for AgNPs synthesis because of its simplicity and its ability to control nanoparticle size and morphology [10]. This method involves the reduction of silver ions in an aqueous medium using trisodium citrate (TSC), which also acts as a stabilizer to prevent aggregation [10]. However, synthesis outcomes depend on multiple parameters, including reaction temperature, silver nitrate concentration, TSC concentration, and the timing of TSC addition [1, 11]. Furthermore, storage conditions also play a crucial role in preserving the long-term stability of AgNPs [11]. Achieving precise control over nanoparticle size and morphology is essential for ensuring reproducible performance in sensing applications [10, 11].

Reaction temperature is one of the most significant factors affecting nucleation and growth. Higher temperatures accelerate nucleation, yielding smaller, more uniform nanoparticles [12, 13], whereas lower temperatures lead to larger, more polydisperse particles because of slower nucleation [12, 14]. TSC, which serves as both a reducing agent and a stabilizer, requires careful concentration control, as insufficient TSC leads to incomplete reduction and aggregation [15], whereas excessive amounts alter

growth kinetics and affect size and morphology [16]. The timing of TSC addition is equally critical, as uncontrolled introduction leads to irregular nucleation and non-uniform nanoparticles. Additionally, precise TSC addition timing is crucial because uncontrolled nucleation during UV-activated synthesis can lead to irregular particle morphology [16, 17].

Previous studies have demonstrated that controlled synthesis parameters can be validated using UV-VIS spectroscopy to track LSPR peaks at approximately 400 nm, which indicate successful nanoparticle formation [16, 18, 19]. Complementary characterization techniques, including FESEM and EDX, provide morphological and elemental analysis, while DLS and zeta potential measurements assess particle size and colloidal stability [18, 19].

This study aims to optimize AgNP synthesis by systematically evaluating the influence of TSC addition timing, reaction temperature, TSC concentration, and storage conditions. By optimizing these synthesis parameters, this research supports the development of highly stable AgNPs.

2. METHODOLOGY

The overall experimental workflow is summarized in Figure 1, outlining the sequential steps from AgNPs synthesis to characterization.

2.1. Materials

Silver nitrate ($AgNO_3$, 99.99% trace metals basis, Sigma-Aldrich) was used as the silver precursor, while trisodium citrate dihydrate (TSC, $Na_3C_6H_5O_7{\cdot}2H_2O$, ACS reagent, ≥ 99.0%, Fisher Scientific) served as both a reducing and stabilizing agent. Deionized (DI) water was used as the solvent for all experimental procedures.

2.2. Synthesis of Silver Nanoparticles (AgNPs)

AgNPs were synthesized using the Turkevich method to investigate the effects of TSC addition timing, storage conditions, reaction temperature, and TSC concentration on nanoparticle formation, as presented in Table 1 and Figure 2, in two batches as follows:

- **Batch 1:** Influence of TSC Addition Timing and Storage Conditions on AgNP Formation
- **Batch 2:** Influence of TSC Concentration and Reaction Temperature on AgNPs Formation

In Batch 1, the influence of TSC addition timing and subsequent storage conditions was investigated. Solution A was heated to 90°C with stirring at 900 rpm, and a fixed volume of Solution B (1.6 mL, 0.2 g [0.054 mM TSC]) was added either at 90°C or at the start of heating. The resulting samples are listed in Table 2.

In Batch 2, the influence of TSC concentration and reaction temperature was investigated. In this batch, Solution A was heated to 70°C, 80°C, or 90°C with stirring at 900 rpm. For each temperature, 1.6 mL of Solution B with varying TSC concentrations of 0.5 g (0.136 mM), 1.0 g (0.272 mM), and 1.5 g (0.408 mM) was added, producing a total of nine samples that were stored in airtight amber bottles at room temperature, as listed in Table 3.

The synthesis parameters in these two batches were selected to study how key chemical and thermal factors influence AgNPs formation in the Turkevich method. Batch 1 focused on the effect of TSC addition timing and storage conditions on nucleation and post-synthesis stability, allowing comparison between early- and late-stage reduction pathways. Batch 2 examined how reaction temperature (70°C, 80°C, 90°C) and TSC concentration influence reduction kinetics, particle size, and colloidal

Table 1. Experimental summary for AgNPs synthesis

Procedure	Batch 1	Batch 2
Preparation of Solution A (0.06mM $AgNO_3$)	1) 0.034 g of $AgNO_3$ was dissolved into 40 mL of DI water 2) 20 mL of dissolved solution was diluted into 100 mL of DI water 3) 60 mL of diluted solution was transferred into a conical flask	
Preparation of Solution B	The following TSC concentration was dissolved into 20 mL of DI water: • 0.2 g (0.054 mM)	The following TSC concentration was dissolved into 20 mL of DI water (separately): • **Concentration 1**: 0.5 g (0.136 mM) • **Concentration 2**: 1.0 g (0.272 mM) • **Concentration 3**: 1.5 g (0.408 mM)
Heating and TSC Addition	1) Solution A was heated while stirring at 900 rpm 2) 1.6 mL of Solution B was added as follows: • **Sample 1** and **Sample 2a**: At 90°C • **Sample 2b**: At the start of heating	1) Solution A was heated while stirring at 900 rpm 2) 1.6 mL of Solution B (Concentration 1) was added at the following temperatures: • **Temperature 1**: 70°C • **Temperature 2**: 80°C • **Temperature 3**: 90°C 3) Steps 1 and 2 were repeated for Concentration 2 and Concentration 3
Observation of Color Change	A pale yellow to greyish color was observed, indicating AgNPs formation	
Storage	The samples were stored in an amber bottle and kept as follows: • **Sample 1**: Cool storage (~4°C) • **Sample 2a** and **Sample 2b**: Room storage (~25°C)	The samples were stored in an amber bottle and kept in room storage (~25°C)

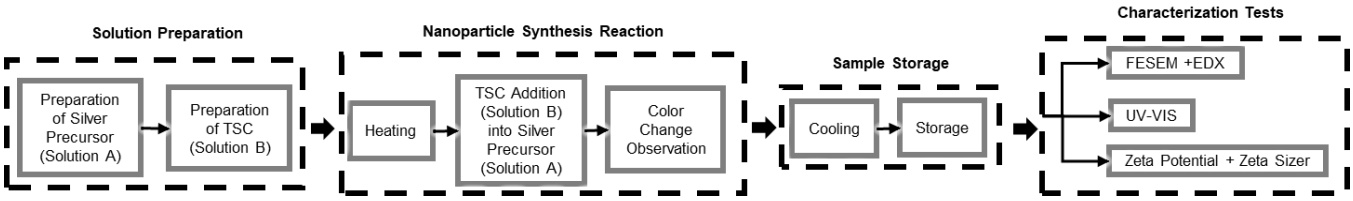

Figure 1. Block diagram illustrating the AgNPs synthesis protocol followed by a sequence of characterization tests

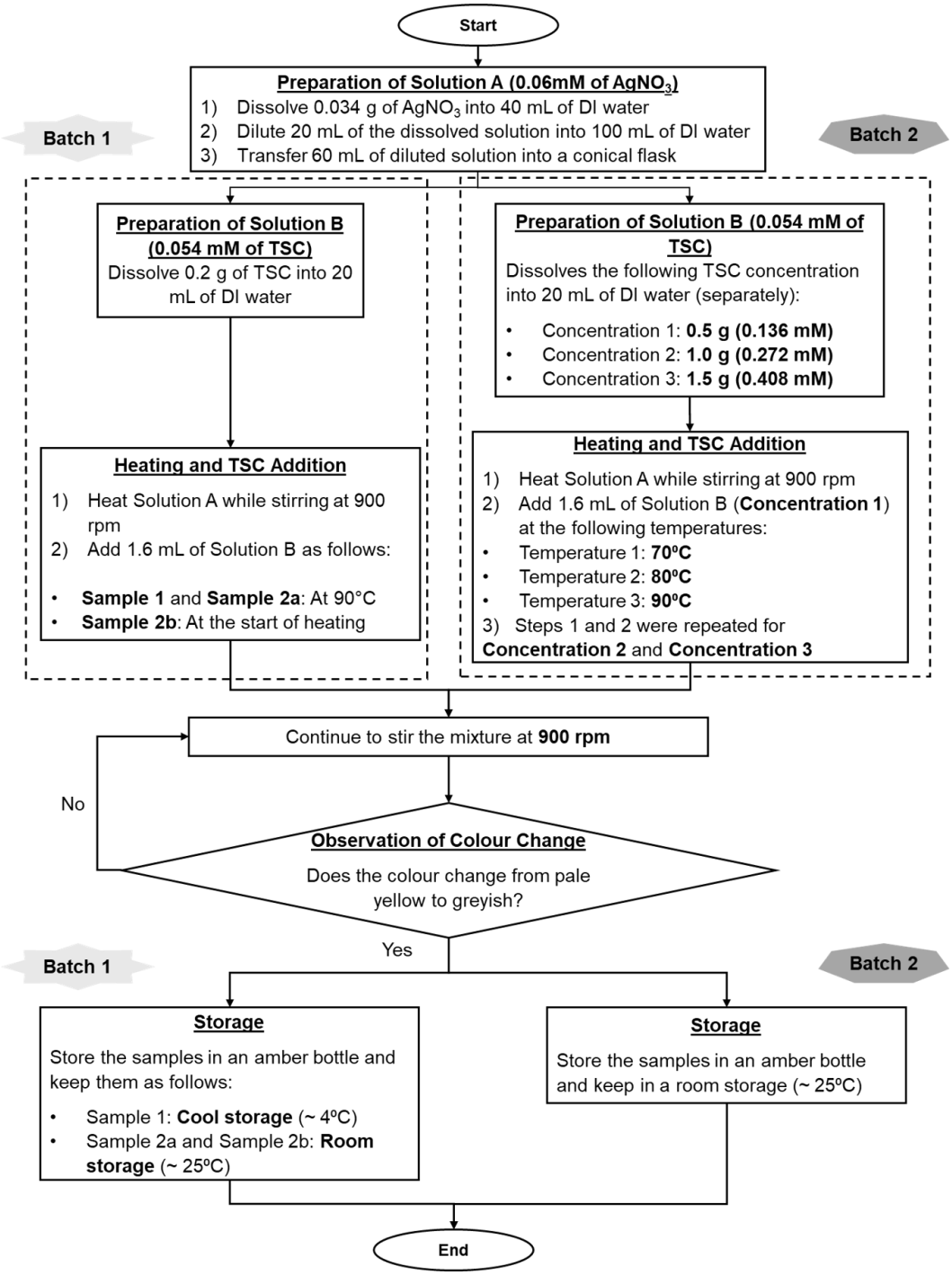

Figure 2. Schematic flow diagram of AgNPs synthesis, highlighting parameter variations between Batch 1 and Batch 2

stability, highlighting the balance between nucleation rate and particle growth. The range of TSC concentrations also enables evaluation of citrate's dual role as a reducing and stabilizing agent in controlling particle uniformity. Storage conditions in Batch 1 were included to monitor oxidation or aggregation over time, providing insight into post-synthesis behavior. Together, these controlled variations provide a structured basis for identifying synthesis conditions that produce uniform, reproducible, and highly stable AgNPs suitable for further characterization and application.

Table 2. List of samples for Batch 1: Influence of TSC Addition Timing and Storage Condition of AgNPs Formation

Sample Name	Description
Sample 1	AgNPs with TSC 0.2 g (0.054 mM) added at 90°C with cool storage (~4°C)
Sample 2a	AgNPs with TSC 0.2 g (0.054 mM) added at 90°C with room temperature storage (~25°C)
Sample 2b	AgNPs with TSC 0.2 g (0.054 mM) added at the start of heating with room temperature storage (~25°C)

Table 3. List of samples for Batch 2: Influence of TSC Concentration and Reaction Temperature on AgNPs Formation

Sample Name	Description
Sample 1	AgNPs with TSC 0.5g (0.136 mM) added at 70°C
Sample 2	AgNPs with TSC 0.5g (0.136 mM) added at 80°C
Sample 3	AgNPs with TSC 0.5g (0.136 mM) added at 90°C
Sample 4	AgNPs with TSC 1.0g (0.272 mM) added at 70°C
Sample 5	AgNPs with TSC 1.0g (0.272 mM) added at 80°C
Sample 6	AgNPs with TSC 1.0g (0.272 mM) added at 90°C
Sample 7	AgNPs with TSC 1.5g (0.408 mM) added at 70°C
Sample 8	AgNPs with TSC 1.5g (0.408 mM) added at 80°C
Sample 9	AgNPs with TSC 1.5g (0.408 mM) added at 90°C

2.3. Characterization of AgNPs

The synthesized AgNPs were characterized to evaluate their morphological, optical, and colloidal stability properties. For Batch 1, the samples were drop-cast onto cleaned glass substrates and incubated for 48 hours to observe the morphology and distribution of AgNPs using Field Emission Scanning Electron Microscopy (FESEM), while Energy Dispersive X-ray Spectroscopy (EDX) confirmed the elemental composition, particularly the presence of silver. For Batch 2, additional characterization techniques were used to assess particle size, optical properties, and stability. UV-Visible Spectroscopy (UV-Vis, 300 – 700 nm) was used to identify the surface plasmon resonance (SPR) peak, indicating the formation of AgNPs. Zeta Potential analysis measured the surface charge and colloidal stability of the nanoparticles, while DLS measurements performed using a Zeta Sizer instrument provided insight into their hydrodynamic diameter and size distribution. Both measurements were recorded in triplicate for each sample to ensure statistical consistency. These complementary techniques enabled a thorough evaluation of AgNP uniformity, aggregation, and optical properties, ensuring reproducible and reliable synthesis outcomes for sensing applications.

3. RESULTS AND DISCUSSION

The following subsections present and discuss the findings, highlighting trends in nanoparticle formation, stability, and aggregation for the samples produced in Batch 1 and Batch 2.

3.1. Batch 1: Influence of TSC Addition Timing and Storage Conditions on AgNPs Formation

The results from Batch 1 show that the timing of TSC addition strongly influences nucleation behavior, with TSC addition at 90°C typically yielding smaller and more uniformly distributed nanoparticles. In contrast, adding TSC at the start of heating exposed the precursor to a slower reduction environment, often leading to broader size distributions or early-stage aggregation. Storage conditions further contributed to stability differences, with cool storage mitigating agglomeration relative to room temperature. These trends were supported by FESEM observations of particle morphology, while EDX confirmed the elemental identity and purity of the synthesized nanoparticles.

3.1.1. Morphological Analysis via FESEM

FESEM was used to analyze the morphology and size distribution of AgNPs synthesized under different TSC addition timings and storage conditions. The FESEM images in Figure 3 show clear variations in particle visibility and uniformity across the three samples. To support the visualization of particle size differences, a bar graph is provided in Figure 4, summarizing the representative nanoparticle size measurements for each sample and highlighting their relative differences under the tested synthesis conditions.

Sample 1 (Batch 1) exhibited distorted and blurry features, making it difficult to identify individual nanoparticles, likely because of poor dispersion, agglomeration, or charging effects during imaging. In the next two samples, the image quality improved significantly, allowing the nanoparticles to be identified. In Sample 2a, the average particle size was approximately 77.22 nm, indicating that room-temperature storage enhanced stability and image clarity. In Sample 2b, the particle sizes ranged from 72.91 nm to 90.38 nm. However, the broader size distribution suggests that adding TSC at the start of heating resulted in less controlled nucleation and growth.

Overall, the results indicate that adding TSC precisely at 90°C (Sample 2a) produced more uniform and well-dispersed AgNPs. This aligns with previous studies in which controlled TSC addition during synthesis at a higher temperature (90°C) improved nucleation and particle uniformity [20–22]. Furthermore, the use of TSC as both a reducing and stabilizing agent plays a crucial role in controlling the size and stability of the synthesized AgNPs [23, 24]. Citrate ions adsorbed onto the surface of the nanoparticles act as a protective layer, preventing agglomeration through electrostatic repulsion [25]. Additionally, AgNPs stored at room temperature under dark conditions maintained their colloidal stability, reducing the risk of aggregation compared with storage at lower temperatures [26–29]. Thus, the synthesis route in Sample 2a offers a simplified and effective approach for obtaining stable, uniform AgNPs.

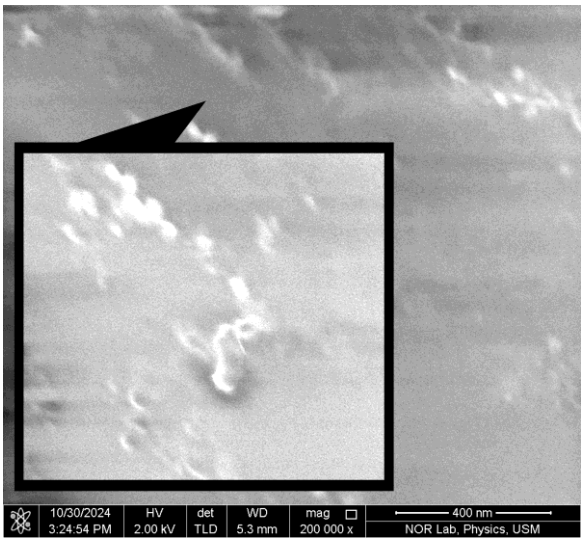

(a)

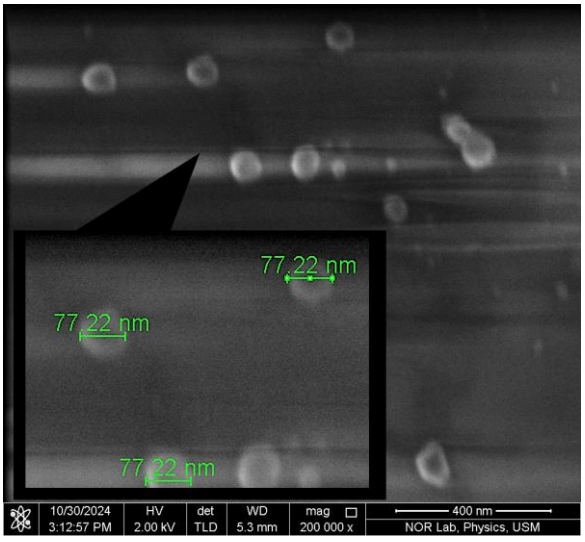

(b)

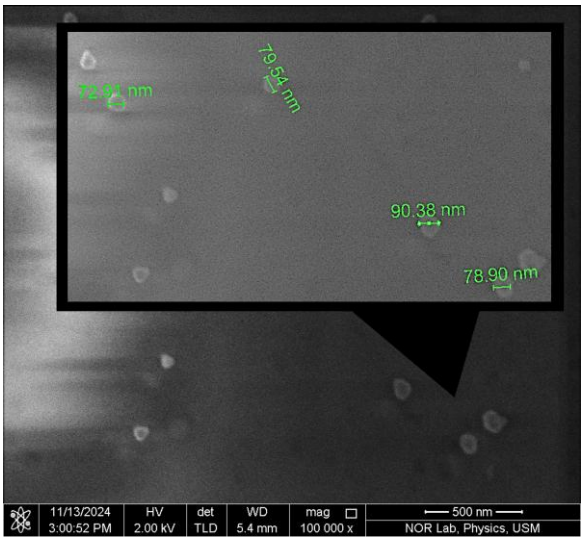

(c)

Figure 3. FESEM images in Batch 1, (a) Sample 1: AgNPs with TSC 0.2 g (0.054 mM) added at 90°C with cool storage (~4°C), (b) Sample 2a: AgNPs with TSC 0.2 g (0.054 mM) added at 90°C with room temperature storage (~25°C), (c) Sample 2b: AgNPs with TSC 0.2 g (0.054 mM) added at the start of heating with room temperature storage (~25°C)

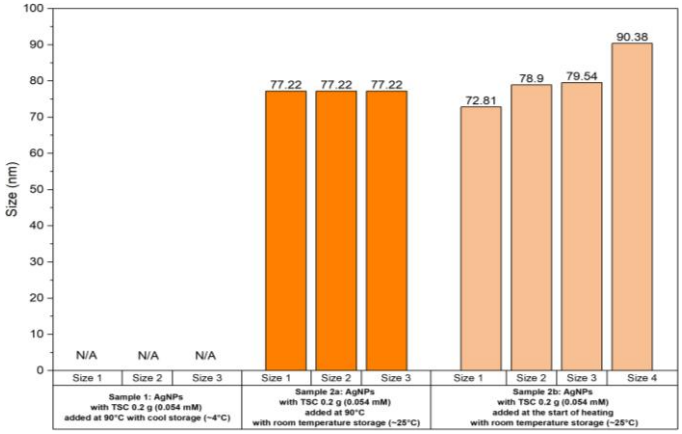

Figure 4. Particle size comparison of AgNPs samples produced in Batch 1

3.1.2. Elemental Composition via EDX

EDX was used to determine the elemental composition of the synthesized AgNPs and to support FESEM observations. Figure 5 and Figure 6 present the atomic percentage (at%) and the weight percentage (wt%) compositions, respectively. The key elements detected included silver (Ag), oxygen (O), sodium (Na), magnesium (Mg), silicon (Si), and calcium (Ca), with Ag being the primary target element, whereas O and Si originate mainly from the glass substrate.

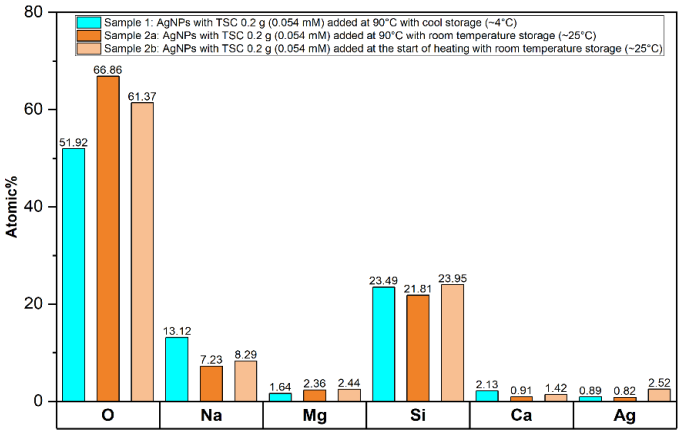

Figure 5. Comparison of EDX elemental composition (at%) of AgNPs synthesized with 0.2g TSC under different conditions

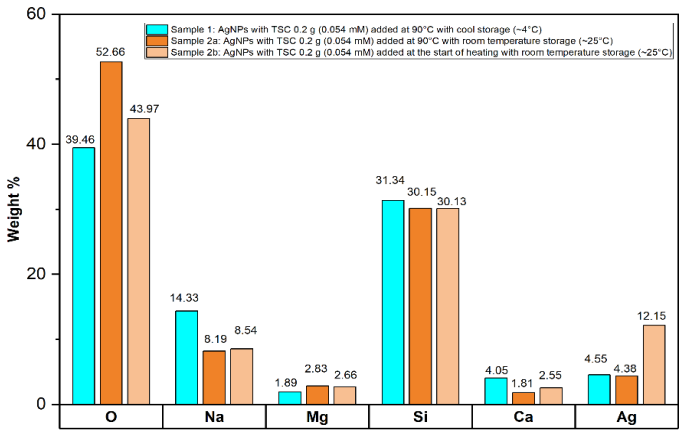

Figure 6. Comparison of EDX elemental composition (wt%) of AgNPs synthesized with 0.2g TSC under different conditions

Sample 1 (Batch 1) showed an Ag content of 0.89 at% and 4.55 wt%, indicating the presence of AgNPs, although FESEM imaging was distorted, limiting morphological interpretation. Sample 2a contained 0.82 at% and 4.38 wt% Ag, slightly lower than Sample 1, yet FESEM revealed clearer particle visibility. Sample 2b displayed a substantially higher Ag content (2.52 at% and 12.15 wt%), suggesting a greater presence of AgNPs. This aligns with FESEM observations, in which Sample 2b exhibited larger and more aggregated nanoparticles, contributing to stronger Ag signals within the EDX sampling area.

The elevated O and Si contents in Samples 1 and 2a reflect contributions from the glass substrate and possible surface oxidation. The relatively lower O content and higher Ag content in Sample 2b support the interpretation that early TSC addition promotes the formation of larger or more continuous Ag domains, consistent with its broader size distribution observed in FESEM. These variations illustrate how TSC addition timing affects the distribution and aggregation of AgNPs during synthesis.

Overall, Sample 2a remains the preferred synthesis route due to its precise TSC addition at 90°C combined with room temperature, which resulted in controlled nucleation and particle growth, preventing random aggregation that may occur with uncontrolled addition timing [30, 31]. This approach provides stable, reproducible AgNPs while maintaining a practical and simplified synthesis procedure.

3.2. Batch 2: Influence of TSC Concentration and Reaction Temperature on AgNPs Formation

The results from Batch 2 are presented to evaluate the influence of reaction temperature and variation in TSC concentration on AgNP formation. UV-VIS spectroscopy was used to analyze the optical properties of the nanoparticles, while Zeta Potential and Zeta Sizer measurements assessed colloidal stability and hydrodynamic size distribution. FESEM and EDX analyses were performed on selected samples to examine surface morphology and elemental composition. Together, these characterization methods were used to identify the synthesis conditions that yield stable, uniform, and well-formed AgNPs.

3.2.1. Optical Properties via UV-VIS Spectroscopy

The UV-VIS absorbance spectra shown in Figure 7 were used to analyze the optical properties of AgNPs synthesized at different temperatures and concentrations, while Table 4 presents the corresponding SPR peak positions. The SPR peak is highly sensitive to particle size, shape, and dispersion, making UV–VIS a reliable preliminary indicator of formation efficiency and nanoparticle quality. Variations in peak intensity and wavelength provide insights into nucleation behavior, growth dynamics, and the degree of colloidal stability achieved during synthesis. The spectra reveal clear trends in nanoparticle formation as a function of reaction conditions, allowing direct comparison of temperature- and concentration-dependent effects.

Table 4. SPR peak wavelengths of synthesized AgNPs samples in Batch 2

Sample Name	SPR Peak (nm)
Sample 1	269
Sample 2	436–469
Sample 3	348–510
Sample 4	272
Sample 5	432
Sample 6	350–496
Sample 7	269
Sample 8	446
Sample 9	349–519

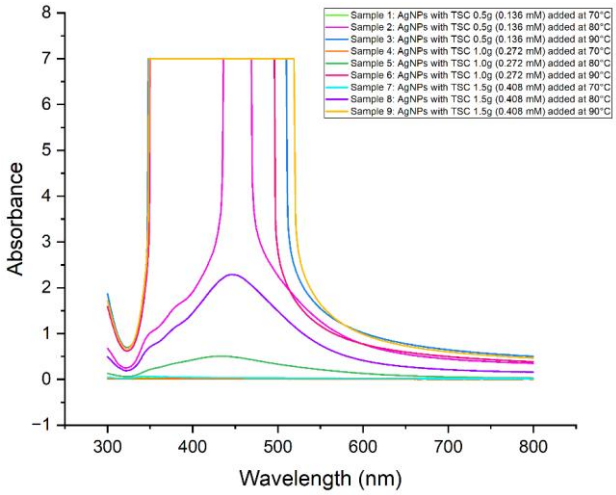

Figure 7. Comparison of UV-VIS absorbance spectra for all synthesized AgNPs samples in Batch 2

At 70°C, the absorbance values remained relatively low across all samples (Sample 1, Sample 4, and Sample 7), with peaks observed around 269–272 nm. This suggests minimal nanoparticle formation or early-stage nucleation with limited growth. SPR peaks emerged at 80°C (Sample 2, Sample 5, and Sample 8), appearing within 432–469 nm and accompanied by higher absorbance. The peak redshift and higher intensity indicate larger particle formation compared with 70°C. At 90°C, all samples (Sample 3, Sample 6, and Sample 9) showed substantially higher absorbance and broader SPR bands in the range of 348–519 nm. The increased peak intensity reflects higher nanoparticle yield, whereas peak broadening indicates a wider particle size distribution and enhanced growth dynamics.

Overall, increasing the synthesis temperature resulted in a redshift of the SPR peak, consistent with the formation of larger AgNPs. Higher TSC concentrations further enhanced absorbance intensity, indicating improved reduction efficiency and greater nanoparticle yield. Based on the UV-VIS results, 80°C and 90°C appear to be more suitable for AgNP synthesis, as they exhibit well-defined SPR peaks within the expected range for stable AgNPs (>400 nm) [32–35].

3.2.2. Particle Stability and Size via Zeta Potential and Zeta Sizer

The stability of AgNPs in suspension is significantly influenced by their surface charge, which can be assessed using Zeta Potential measurements. Higher absolute Zeta Potential values (typically above ±30 mV) indicate stronger electrostatic repulsion and enhanced colloidal stability. Particle size distribution was analyzed using the Zeta Sizer, which provides hydrodynamic diameter measurements. To ensure accuracy and reproducibility, three consecutive measurements (M1, M2, M3) were taken for both Zeta Potential and Zeta Sizer for each sample, and the comparative results for each parameter are presented graphically with corresponding error bars. The mean and standard deviation (SD) values are summarized in the accompanying tables for clarity.

Figure 8 presents the Zeta Potential values of all Batch 2 samples, highlighting the influence of reaction temperature and TSC concentration on nanoparticle stability. Measurement variability is further illustrated in Figure 9 using error bars, while Table 5 provides the corresponding mean with SD for each sample.

Across all TSC concentrations, AgNPs synthesized at higher temperatures (80°C and 90°C) consistently exhibited more negative Zeta Potential values than those synthesized at 70°C, indicating stronger electrostatic repulsion and better colloidal stability. In contrast, samples at 70°C displayed relatively less negative values, reflecting weaker repulsive forces and a higher tendency for aggregation. The concentration of TSC also strongly influenced colloidal stability. At the lower TSC concentration of 0.5 g (0.136 mM), the AgNPs exhibited relatively unstable characteristics, particularly those synthesized at 70°C, with Zeta Potential values of –6.32 to –7.02 mV, indicating a high risk of aggregation. Increasing the TSC concentration to 1.0 g (0.272 mM) resulted in improved stability, particularly at 80°C and 90°C, where Zeta Potential values reached –30 to –45 mV, suggesting stronger electrostatic repulsion and better dispersion. The highest TSC concentration, 1.5 g (0.408 mM), yielded the most negative values of –45.1 to –49.6 mV, with the strongest response recorded at 80°C, confirming effective prevention of agglomeration. Among all samples, those synthesized at 80°C with 1.5 g TSC exhibited the highest Zeta Potential magnitude (–45 to –49.6 mV), indicating optimal stability.

The Zeta Sizer results, including Z-Average and polydispersity index (PdI), provide key insights into nanoparticle size and dispersion. Figure 10 compares the Z-Average of all samples, with error bars shown in Figure 11 and mean with SD values listed in Table 6. Higher synthesis temperatures (80°C and 90°C) consistently produced smaller nanoparticles compared with 70°C. At 70°C, large particle sizes were observed for TSC concentrations of 1.0–1.5 g (422.2–759.7 nm), indicating incomplete reduction and potential aggregation. In contrast, at elevated temperatures, particle sizes decreased substantially, with the smallest AgNPs obtained at 90°C for 1.0 g TSC (22.54–22.76 nm) and 1.5 g TSC (27.41–28.47 nm), reflecting enhanced nucleation and controlled growth.

Figure 12 presents the PdI of all samples, reflecting the uniformity of the particle size distribution. Figure 13 illustrates the error bars, and Table 7 summarizes the mean and SD values, supporting the identification of samples with the most monodispersed nanoparticle populations. Lower PdI values (<0.5) indicate narrower size distributions and better nanoparticle uniformity [36]. The most monodispersed AgNPs were observed at 80°C for TSC

Table 5. Mean Zeta Potential with SD for Samples 1–9

Sample Name	Mean of Zeta Potential (mV)	Standard deviation
Sample 1	-6.65	0.35
Sample 2	-42	2.26
Sample 3	-45.23	2.21
Sample 4	-32.83	1.48
Sample 5	-30.6	0.35
Sample 6	-44.17	2.11
Sample 7	-36.8	1.47
Sample 8	-47.27	2.25
Sample 9	-42.37	0.87

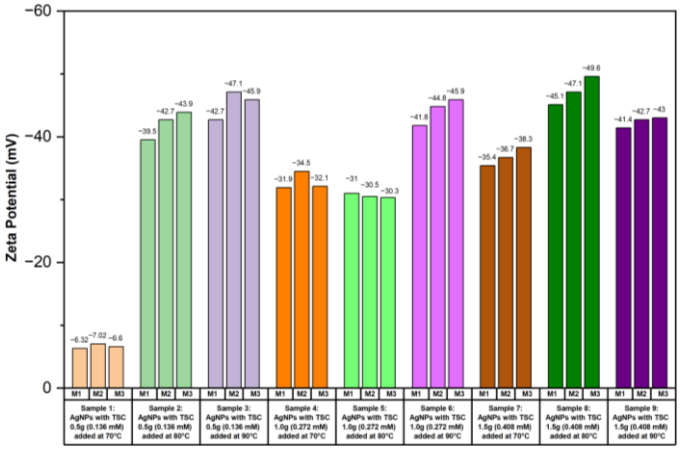

Figure 8. Comparison of Zeta Potential for all synthesized AgNPs samples in Batch 2

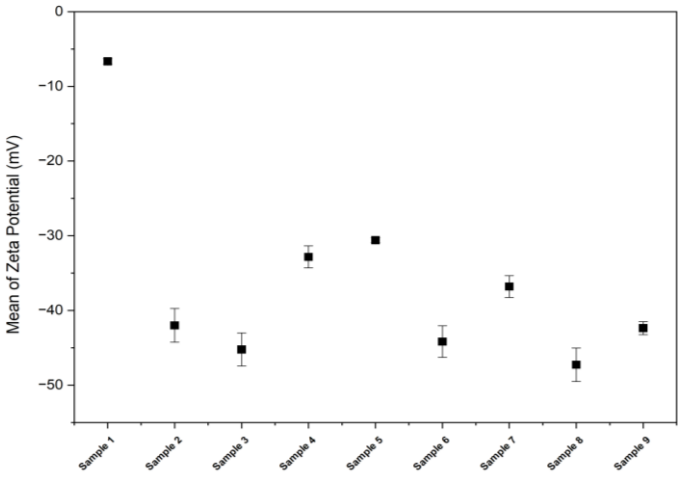

Figure 9. Zeta Potential error bars for Samples 1–9

concentrations of 0.5 g (PdI ~0.30) and 1.5 g (PdI ~0.43), reflecting stable suspensions with minimal size variation. Higher PdI values (>0.5), such as those for 1.0 g TSC (0.272 mM) at 70°C, ranged around 0.542 to 0.794, reflecting a broad size distribution due to uncontrolled particle growth and aggregation. Notably, 0.5 g TSC (0.136 mM) at 90°C exhibited small particle sizes within 26.42–26.58 nm but a moderate PdI of around 0.544–0.553, indicating that efficient size reduction can still coexist with moderate polydispersity.

Overall, the findings show that synthesis temperatures of 80°C and above consistently produce smaller and more stable AgNPs, while increasing the TSC concentration improves size uniformity and reduces aggregation. Reaction temperature and TSC concentration are dominant factors in AgNP synthesis, with higher temperatures promoting faster nucleation and smaller, more stable nanoparticles, while increased TSC levels enhance electrostatic stabilization, ensuring uniform and well-dispersed AgNPs [37–40].

Table 6. Mean Z-Average with SD for Samples 1–9

Sample Name	Mean of Z-Average (d.nm)	Standard deviation
Sample 1	248.63	47.47
Sample 2	47.2	0.04
Sample 3	26.51	0.08
Sample 4	600.7	138.24
Sample 5	33.03	0.22
Sample 6	22.59	0.15
Sample 7	479.07	57.25
Sample 8	38.94	0.23
Sample 9	27.78	61.87

Table 7. Mean PdI with SD for Samples 1–9

Sample Name	Mean of PdI	Standard deviation
Sample 1	0.31	0.01
Sample 2	0.30	0.00
Sample 3	0.55	0.00
Sample 4	0.63	0.14
Sample 5	0.57	0.00
Sample 6	0.53	0.00
Sample 7	0.49	0.07
Sample 8	0.44	0.01
Sample 9	0.52	0.04

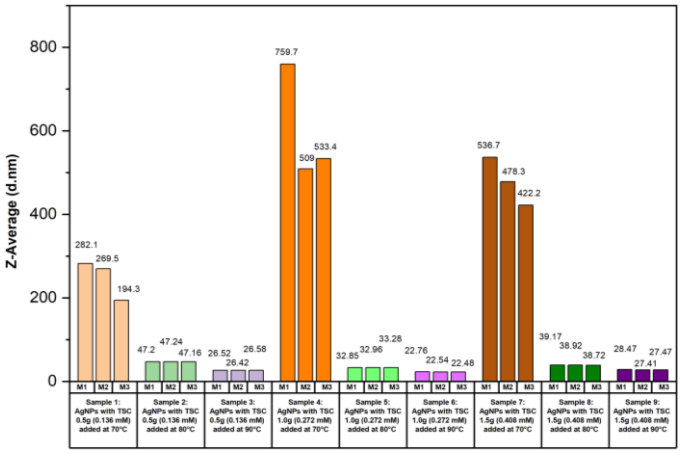

Figure 10. Comparison of Z-Average for all synthesized AgNPs samples in Batch 2

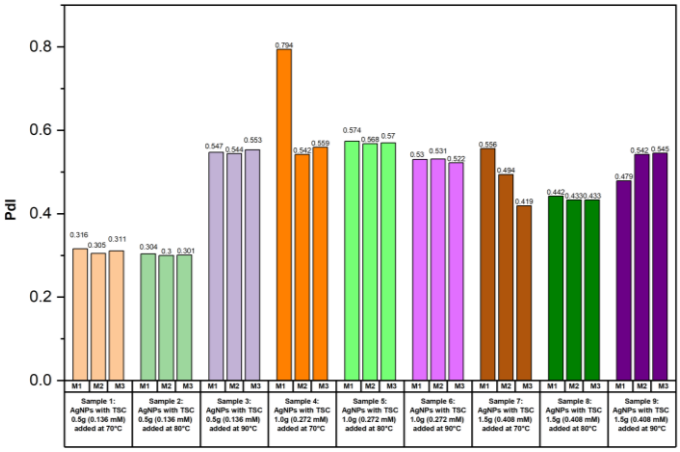

Figure 12. Comparison of PdI in Zeta Sizer for all synthesized AgNPs samples in Batch 2

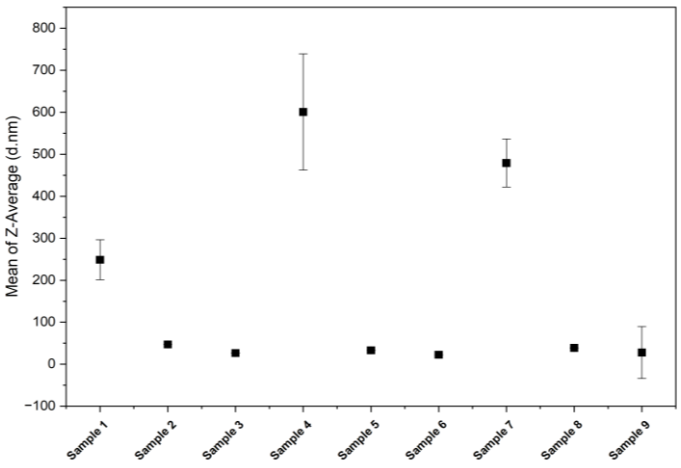

Figure 11. Z-Average bars for Samples 1–9

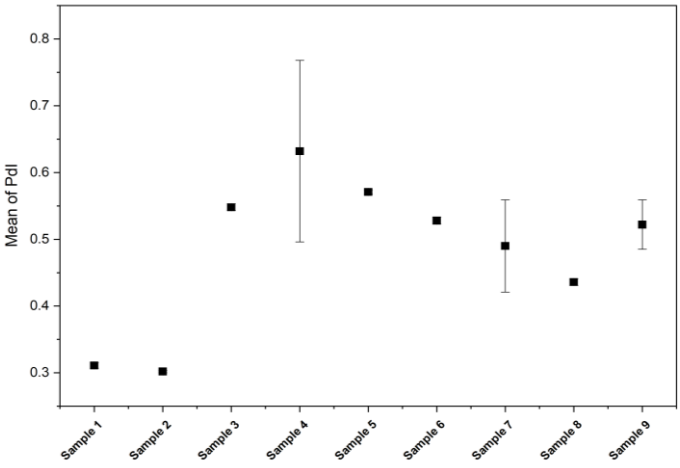

Figure 13. PdI error bars for Samples 1–9

3.2.3. Morphological and Elemental Analysis via FESEM-EDX

The morphology and elemental composition of AgNPs synthesized at 90 °C with varying TSC concentrations were analyzed using FESEM and EDX. Based on the UV-VIS and Zeta analysis results, Sample 3, Sample 6, and Sample 9 were selected for further characterization because of their well-defined SPR peaks and high colloidal stability. The FESEM images in Figure 14 confirm the presence of nanoparticles in all three samples, although some regions appear slightly blurry, likely because of charging effects. Despite this, the nanoparticles remained distinguishable, and differences in size and dispersion are further illustrated in the bar graph presented in Figure 15.

In Sample 3, the AgNPs appeared larger and slightly more polydisperse, at 74.92–79.59 nm, indicating weaker surface stabilization and minor aggregation, likely due to weaker steric hindrance from the lower amount of TSC. Increasing the TSC concentration produced smaller and more uniformly distributed nanoparticles. Sample 6 and Sample 9 exhibited narrower size ranges of 72.85–78.68 nm and 72.85–78.68 nm, respectively, reflecting stronger stabilization at higher citrate levels. This behavior aligns with previous studies in which increased TSC concentrations led to smaller and more stable nanoparticles [16, 41]. The stabilizing effect of TSC is attributed to its dual mechanism: electrostatic repulsion, in which negatively charged citrate ions prevent particle aggregation, and steric stabilization through the formation of a protective layer around AgNPs [16, 41]. These findings confirm that optimizing TSC concentration and addition timing is crucial for achieving well-dispersed AgNPs.

The particle sizes obtained from Zeta Sizer and FESEM are compared in Table 8. Zeta Sizer measurements showed much smaller Z-Average values, around 22.48–28.7 nm, compared with both Peak 1 values of 55.97–66.42 nm and FESEM results of around 72.85–79.59 nm. This difference arises because the Z-Average is an intensity-weighted mean that includes all scattering populations, including smaller particles and minor aggregates, and therefore often underestimates the true dominant size. In contrast, Peak 1 better represents the primary nanoparticle population and aligns more closely with FESEM measurements, indicating its reliability in reflecting the actual nanoparticle size in solution.

The larger sizes observed in FESEM can be attributed to the absence of the solvation layer, which is present in Zeta Sizer measurements, as well as possible particle aggregation during drying and surface interactions with the substrate. Because FESEM provides direct visualization in a dry state, nanoparticles may appear larger than their hydrated counterparts in solution.

The slightly larger dimensions observed in FESEM can be attributed to the absence of the solvation layer present in Zeta Sizer measurements, as well as possible particle clustering during the drying stage prior to imaging. Since FESEM captures nanoparticles in the dry state, sizes naturally appear larger than hydrodynamic diameters measured in solution.

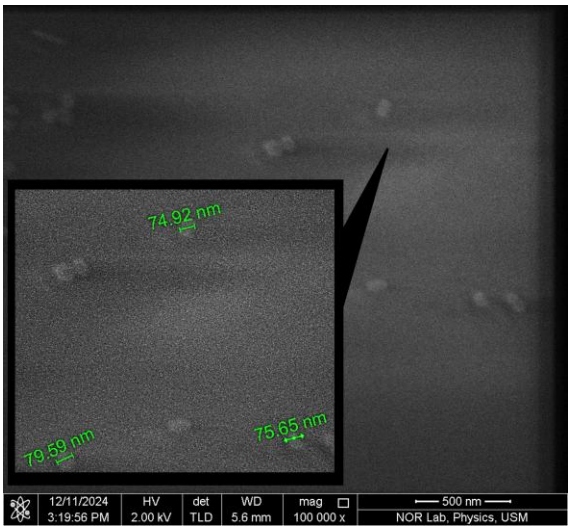

(a)

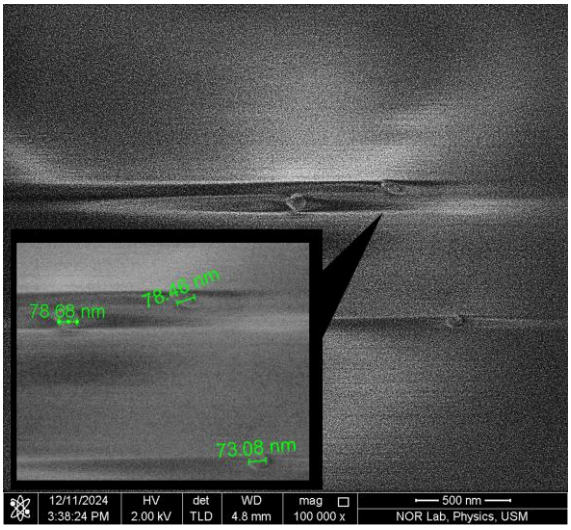

(b)

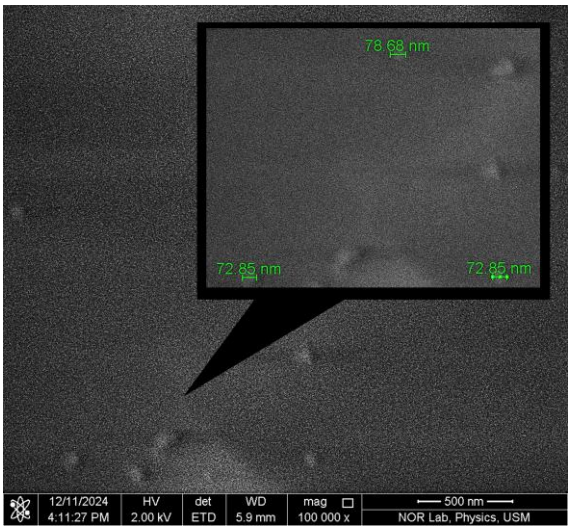

(c)

Figure 14. FESEM images in Batch 2, (a) Sample 3: AgNPs with TSC 0.5 g (0.136 mM) added at 90°C, (b) Sample 6: AgNPs with TSC 1.0 g (0.272 mM) added at 90°C, (c) Sample 9: AgNPs with TSC 1.5 g (0.408 mM) added at 90°C

Table 8. Comparison of Zeta Sizer and FESEM measurements of Sample 3, Sample 6 and Sample 9 in Batch 2

Sample Name	Zeta Sizer (d.nm)						FESEM
	Z-Average 1	Peak 1	Z-Average 2	Peak 1	Z-Average 3	Peak 1	
Sample 3	26.52	63.53	26.42	66.42	26.58	62.57	74.92–79.59 nm
Sample 6	22.76	57.77	22.54	57.96	22.48	55.97	73.08–78.68 nm
Sample 9	28.47	62.13	27.41	62.17	27.47	61.31	72.85–78.68 nm

EDX analysis shown in Figure 16 and Figure 17 confirmed the presence of silver (Ag), oxygen (O), sodium (Na), magnesium (Mg), and silicon (Si) in the selected samples. The distribution of these elements varies depending on the TSC concentration, which affects nanoparticle formation and surface coverage.

Sample 3 recorded the highest Ag at% (3.52%) and wt% (16.97%), indicating a high surface concentration of silver nanoparticles, which is commonly associated with the formation of larger or more aggregated particles that appear more prominently in EDX analysis. In contrast, Sample 6 exhibited a moderate Ag at% (1.51%) and wt% (8.11%), reflecting a reduction in surface Ag content. This outcome aligns with the effect of increased TSC concentration, which promotes the formation of smaller and more uniformly dispersed nanoparticles, thereby lowering the detectable Ag signal. Sample 9 showed the lowest Ag at% (0.8%) and wt% (4.41%), suggesting a significant decrease in Ag detection. The stronger capping effect of excess TSC likely resulted in the formation of smaller nanoparticles, further reducing Ag detection in EDX because of the more uniform and well-dispersed nanoparticle distribution.

Most samples contained O and Si, primarily from the glass substrate, with oxygen increasing slightly as TSC concentration increased, possibly because of stronger citrate coverage. Na was present in small amounts, likely from residual precursor salts, while Mg appeared only in trace quantities, suggesting that it may be an impurity from the reactants or synthesis environment.

Overall, FESEM-EDX analysis confirms that increasing TSC concentration at 90°C leads to smaller, more uniform, and more effectively stabilized AgNPs. Peak 1 values from the Zeta Sizer showed the strongest correlation with FESEM sizes, validating their use as a reliable indicator of particle size in solution. Meanwhile, EDX results support the observed morphological trends by showing reduced Ag signal intensity as nanoparticles become better capped and more dispersed. These findings emphasize the role of TSC in controlling AgNP size, stability, and surface composition. Increasing TSC concentration enhances AgNP stability and size uniformity, while differences between FESEM and Zeta Sizer measurements can be explained by the presence of the solvation layer in solution and the dry-state visualization provided by FESEM. The EDX analysis further confirms silver composition and the presence of stabilizing agents [16, 17, 31, 42].

Mechanistically, TSC acts both as a stabilizing and capping agent: negatively charged citrate ions induce electrostatic repulsion to prevent aggregation during nucleation, while

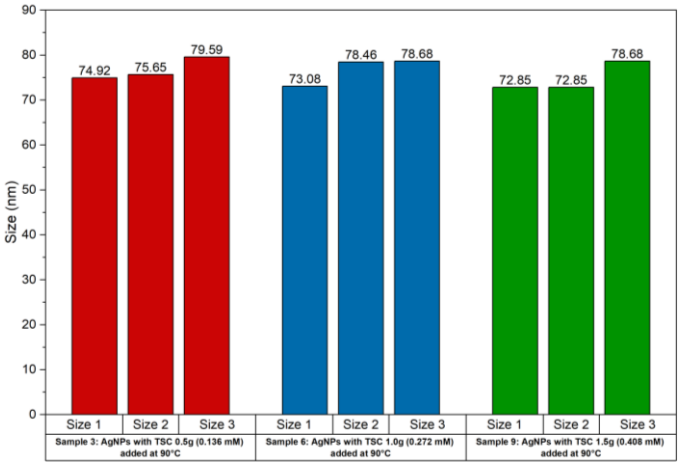

Figure 15. Particle size comparison of AgNPs for Sample 3, Sample 6 and Sample 9 produced in Batch 2

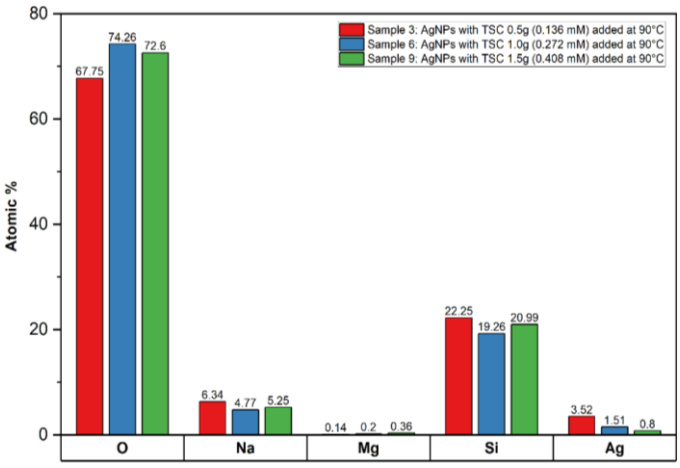

Figure 16. Comparison of EDX elemental composition (at%) of AgNPs synthesized in Sample 3, Sample 6 and Sample 9 in Batch 2

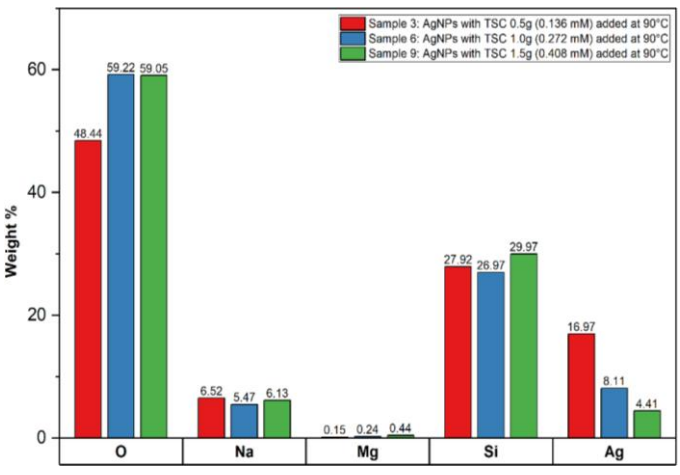

Figure 17. Comparison of EDX elemental composition (wt%) of AgNPs synthesized in Sample 3, Sample 6 and Sample 9 in Batch 2

steric stabilization slows growth and enhances dispersion. Higher TSC concentrations thus favor smaller, more uniform, and stable nanoparticles, consistent with the observed Zeta Potential, PdI, and FESEM-EDX results.

4. CONCLUSION

This study systematically optimized the Turkevich-based synthesis of AgNPs by evaluating the effects of TSC addition timing, storage conditions, reaction temperature, and TSC concentration. The results identify room-temperature storage and TSC addition at 90°C as key parameters for suppressing early-stage agglomeration and ensuring consistent nucleation. Higher reaction temperatures (≥80°C) and increased TSC concentrations (0.136–0.408 mM) produced progressively smaller, more uniform, and more stable AgNPs. These trends were consistently supported across all characterization methods: UV–VIS showed blue-shifted SPR peaks with decreasing particle size, zeta potential increased in magnitude with improved stabilization, and FESEM confirmed uniform morphology at 90°C with 1.0 g TSC. Collectively, this optimized synthesis produced stable, well-dispersed AgNPs with controlled size and morphology. Such attributes are essential for reliable performance in downstream applications, particularly in biosensing, catalysis, and environmental monitoring, where nanoparticle uniformity and stability directly influence sensitivity, reproducibility, and functional efficiency.

ACKNOWLEDGMENTS

The authors gratefully acknowledge the Fundamental Research Grant Scheme (FRGS) [Reference No: FRGS/1/2023/TK07/UITM/02/26] for funding this work. Special appreciation is extended to Universiti Teknologi MARA for providing the necessary facilities and resources. The completion of this research was made possible by the invaluable support of colleagues and laboratory staff for their technical assistance and valuable discussions throughout the study.

REFERENCES

[1] H. I. Badi'ah, F. Seedeh, G. Supriyanto, and A. H. Zaidan, "Synthesis of Silver Nanoparticles and the Development in Analysis Method," *IOP Conference Series: Earth and Environmental Science*, vol. 217, p. 012005, 2019, doi: 10.1088/1755-1315/217/1/012005.

[2] M. W. Juma, Z. Birech, N. M. Mwenze, A. M. Ondieki, M. Maaza, and S. D. Mokhotjwa, "Localized surface plasmon resonance sensing of Trenbolone acetate dopant using silver nanoparticles," *Scientific Reports*, vol. 14, no. 1, p. 5721, 2024, doi: 10.1038/s41598-024-56456-w.

[3] Y. Li, Q. Liao, W. Hou, and L. Qin, "Silver-Based Surface Plasmon Sensors: Fabrication and Applications," *International Journal of Molecular Sciences*, vol. 24, no. 4, p. 4142, 2023, doi: 10.3390/ijms24044142.

[4] L. Wei, J. Lu, H. Xu, A. Patel, Z.-S. Chen, and G. Chen, "Silver nanoparticles: synthesis, properties, and therapeutic applications," *Drug Discovery Today*, vol. 20, no. 5, pp. 595–601, 2015, doi: 10.1016/j.drudis.2014.11.014.

[5] S. H. Lee and B.-H. Jun, "Silver Nanoparticles: Synthesis and Application for Nanomedicine," *International Journal of Molecular Sciences*, vol. 20, no. 4, p. 865, 2019, doi: 10.3390/ijms20040865.

[6] B. Reidy, A. Haase, A. Luch, K. Dawson, and I. Lynch, "Mechanisms of Silver Nanoparticle Release, Transformation and Toxicity: A Critical Review of Current Knowledge and Recommendations for Future Studies and Applications," *Materials*, vol. 6, no. 6, pp. 2295–2350, 2013, doi: 10.3390/ma6062295.

[7] P. Prosposito *et al.*, "Bifunctionalized Silver Nanoparticles as Hg^{2+} Plasmonic Sensor in Water: Synthesis, Characterizations, and Ecosafety," *Nanomaterials*, vol. 9, no. 10, p. 1353, Sep. 2019, doi: 10.3390/nano9101353.

[8] I. Schiesaro *et al.*, "Hydrophilic Silver Nanoparticles for Hg(II) Detection in Water: Direct Evidence for Mercury–Silver Interaction," *The Journal of Physical Chemistry C*, vol. 124, no. 47, pp. 25975–25983, 2020, doi: 10.1021/acs.jpcc.0c06951.

[9] I. Ivanišević, "The Role of Silver Nanoparticles in Electrochemical Sensors for Aquatic Environmental Analysis," *Sensors*, vol. 23, no. 7, p. 3692, 2023, doi: 10.3390/s23073692.

[10] J. Dong, P. L. Carpinone, G. Pyrgiotakis, P. Demokritou, and B. M. Moudgil, "Synthesis of Precision Gold Nanoparticles Using Turkevich Method," *KONA Powder and Particle Journal*, vol. 37, p. 2020011, 2020, doi: 10.14356/kona.2020011.

[11] S. Ibrahim, Z. Ahmad, M. Z. Manzoor, M. Mujahid, Z. Faheem, and A. Adnan, "Optimization for biogenic microbial synthesis of silver nanoparticles through response surface methodology, characterization, their antimicrobial, antioxidant, and catalytic potential," *Scientific Reports*, vol. 11, no. 1, p. 770, 2021, doi: 10.1038/s41598-020-80805-0.

[12] S. S. Muniandy, S. Sasidharan, and H. L. Lee, "Green Synthesis of Ag Nanoparticles and Their Performance towards Antimicrobial Properties," *Sains Malaysiana*, vol. 48, no. 4, pp. 851–860, 2019, doi: 10.17576/jsm-2019-4804-17.

[13] O. Ahmadi, Z. Sayyar, and H. Jafarizadeh Malmiri, "Optimization of Processing Time, Temperature, and Stirring Rate to Synthesize the Ag Nanoparticles Using Oregano Extract," *Iranian Journal of Chemistry and Chemical Engineering*, vol. 42, no. 10, pp. 3235–3248, 2023, doi: 10.30492/ijcce.2023.1971456.5676.

[14] A. N., B. C. Ang, A. M.A., and C. W. Bong, "Influence of Precursor Concentration and Temperature on the Formation of Nanosilver in Chemical Reduction Method," *Sains Malaysiana*, vol. 47, no. 1, pp. 157–168, 2018, doi: 10.17576/jsm-2018-4701-19.

[15] C. Minh Thang Nguyen, Q. Khanh Tran, and V. Tien Nguyen, "Polyol Synthesis of Silver Nanoparticles and Deposition on Carbon Vulcan for 4-Nitrophenol Reduction Catalysis," *Oriental Journal of Chemistry*, vol. 36, no. 1, pp. 139–143, 2020, doi: 10.13005/ojc/360119.

[16] B. Pascu *et al.*, "Silver Nanoparticle Synthesis via Photochemical Reduction with Sodium Citrate," *International Journal of Molecular Sciences*, vol. 24, no. 1, p. 255, 2022, doi: 10.3390/ijms24010255.

[17] O. Velgosova, L. Mačák, E. Čižmárová, and V. Mára, "Influence of Reagents on the Synthesis Process and Shape of Silver Nanoparticles," *Materials*, vol. 15, no. 19, p. 6829, 2022, doi: 10.3390/ma15196829.

[18] J. Vishal, S. Ranjani, R. J. Karunya, and S. Hemalatha, "Synthesis, Characterization and Evaluation of Antioxidant, Anticancer and Toxicity Properties of Silver Nanoparticles Synthesized from Syzygium Aromaticum," *Archives of Breast Cancer*, pp. 291–300, 2023, doi: 10.32768/abc.2023103291-300.

[19] A. K. Bishoyi *et al.*, "Unveiling the antibacterial and antifungal potential of biosynthesized silver nanoparticles from Chromolaena odorata leaves," *Scientific Reports*, vol. 14, no. 1, p. 7513, 2024, doi: 10.1038/s41598-024-57972-5.

[20] S. Agnihotri, S. Mukherji, and S. Mukherji, "Size-controlled silver nanoparticles synthesized over the range 5–100 nm using the same protocol and their antibacterial efficacy," *RSC Advances*, vol. 4, no. 8, pp. 3974–3983, 2014, doi: 10.1039/C3RA44507K.

[21] M. Rozalen, M. Sánchez-Polo, M. Fernández-Perales, T. J. Widmann, and J. Rivera-Utrilla, "Synthesis of controlled-size silver nanoparticles for the administration of methotrexate drug and its activity in colon and lung cancer cells," *RSC Advances*, vol. 10, no. 18, pp. 10646–10660, 2020, doi: 10.1039/C9RA08657A.

[22] S. Roy and T. K. Das, "Synthesis and standardization of biologically synthesized silver nanoparticles," *AIP Conference Proceedings*, vol. 1536, no. 1, pp. 39–40, 2013, doi: 10.1063/1.4810089.

[23] K. Nathanael, S. Cheng, N. M. Kovalchuk, R. Arcucci, and M. J. H. Simmons, "Optimization of microfluidic synthesis of silver nanoparticles: A generic approach using machine learning," *Chemical Engineering Research and Design*, vol. 193, pp. 65–74, 2023, doi: 10.1016/j.cherd.2023.03.007.

[24] L. Mačák, "Synthesis of Differently Shaped Nontoxic AgNPs Stabilized by PVP and TSC," *Evolutions in Mechanical Engineering*, vol. 5, no. 3, 2024, doi: 10.31031/EME.2024.05.000612.

[25] Y. Zhang, H. Yang, and J. Wu, "Study on low temperature sintering of nano-silver paste," in *Proceedings of the International Symposium on Big Data and Artificial Intelligence*, New York, NY, USA: ACM, 2018, pp. 114–118. doi: 10.1145/3305275.3305298.

[26] N. A. Forbes, T. T. Yuan, and M. N. Desilva, "Silver Nanoparticle Storage Stability in Aqueous and Biological Media," San Antonio, Texas, 2015.

[27] J. M. Gorham, A. B. Rohlfing, K. A. Lippa, R. I. MacCuspie, A. Hemmati, and R. David Holbrook, "Storage Wars: how citrate-capped silver nanoparticle suspensions are affected by not-so-trivial decisions," *Journal of Nanoparticle Research*, vol. 16, no. 4, p. 2339, 2014, doi: 10.1007/s11051-014-2339-9.

[28] P. Korshed, L. Li, D.-T. Ngo, and T. Wang, "Effect of Storage Conditions on the Long-Term Stability of Bactericidal Effects for Laser Generated Silver Nanoparticles," *Nanomaterials*, vol. 8, no. 4, p. 218, 2018, doi: 10.3390/nano8040218.

[29] O. Velgosova, P. Varga, D. Ivánová, M. Lisnichuk, and M. Hudá, "Effect of Storage Conditions on the Stability of Colloidal Silver Solutions Prepared by Biological and Chemical Methods," *Metals*, vol. 14, no. 5, p. 513, 2024, doi: 10.3390/met14050513.

[30] S. Agnihotri, S. Mukherji, and S. Mukherji, "Size-controlled silver nanoparticles synthesized over the range 5–100 nm using the same protocol and their antibacterial efficacy," *RSC Advances*, vol. 4, no. 8, pp. 3974–3983, 2014, doi: 10.1039/C3RA44507K.

[31] C. Quintero-Quiroz *et al.*, "Optimization of silver nanoparticle synthesis by chemical reduction and evaluation of its antimicrobial and toxic activity," *Biomaterials Research*, vol. 23, no. 1, 2019, doi: 10.1186/s40824-019-0173-y.

[32] R. Das, S. S. Nath, D. Chakdar, G. Gope, and R. Bhattacharjee, "Synthesis of silver nanoparticles and their optical properties," *Journal of Experimental Nanoscience*, vol. 5, no. 4, pp. 357–362, 2010, doi: 10.1080/17458080903583915.

[33] M. Asif, R. Yasmin, R. Asif, A. Ambreen, M. Mustafa, and S. Umbreen, "Green Synthesis of Silver Nanoparticles (AgNPs), Structural Characterization, and their Antibacterial Potential," *Dose-Response*, vol. 20, no. 2, 2022, doi: 10.1177/15593258221088709.

[34] E. Smiechowicz, B. Niekraszewicz, and P. Kulpinski, "Optimisation of AgNP Synthesis in the Production and Modification of Antibacterial Cellulose Fibres," *Materials*, vol. 14, no. 15, p. 4126, 2021, doi: 10.3390/ma14154126.

[35] S.-W. Lee *et al.*, "Effect of Temperature on the Growth of Silver Nanoparticles Using Plasmon-Mediated Method under the Irradiation of Green LEDs," *Materials*, vol. 7, no. 12, pp. 7781–7798, 2014, doi: 10.3390/ma7127781.

[36] M. Danaei *et al.*, "Impact of Particle Size and Polydispersity Index on the Clinical Applications of Lipidic Nanocarrier Systems," *Pharmaceutics*, vol. 10, no. 2, p. 57, 2018, doi: 10.3390/pharmaceutics10020057.

[37] X.-F. Zhang, Z.-G. Liu, W. Shen, and S. Gurunathan, "Silver Nanoparticles: Synthesis, Characterization, Properties, Applications, and Therapeutic Approaches," *International Journal of Molecular Sciences*, vol. 17, no. 9, p. 1534, 2016, doi: 10.3390/ijms17091534.

[38] X. Jiang, W. Chen, C. Chen, S. Xiong, and A. Yu, "Role of Temperature in the Growth of Silver Nanoparticles Through a Synergetic Reduction Approach," *Nanoscale Research Letters*, vol. 6, no. 1, p. 32, 2010, doi: 10.1007/s11671-010-9780-1.

[39] J. Vega-Baudrit, S. M. Gamboa, E. R. Rojas, and V. V. Martinez, "Synthesis and characterization of silver nanoparticles and their application as an antibacterial agent," *International Journal of*

Biosensors & Bioelectronics, vol. 5, no. 5, 2019, doi: 10.15406/ijbsbe.2019.05.00172.

[40] N. Liaqat, N. Jahan, Khalil-ur-Rahman, T. Anwar, and H. Qureshi, "Green synthesized silver nanoparticles: Optimization, characterization, antimicrobial activity, and cytotoxicity study by hemolysis assay," *Frontiers in Chemistry*, vol. 10, 2022, doi: 10.3389/fchem.2022.952006.

[41] S. Timakwe, B. Silwana, and M. C. Matoetoe, "Electrochemistry as a Complementary Technique for Revealing the Influence of Reducing Agent Concentration on AgNPs," *ACS Omega*, vol. 7, no. 6, pp. 4921–4931, 2022, doi: 10.1021/acsomega.1c05374.

[42] D. Chicea, A. Nicolae-Maranciuc, A. S. Doroshkevich, L. M. Chicea, and O. M. Ozkendir, "Comparative Synthesis of Silver Nanoparticles: Evaluation of Chemical Reduction Procedures, AFM and DLS Size Analysis," *Materials*, vol. 16, no. 15, p. 5244, 2023, doi: 10.3390/ma16155244.